Eur. Phys. J. D **10**, 391–398 (2000)

THE EUROPEAN PHYSICAL JOURNAL D

EDP Sciences

Simulation of Raman spectra of C_{60} and C_{70} by non-orthogonal tight-binding molecular dynamics

T.A. Beu[a], J. Onoe, and K. Takeuchi

The Institute of Physical and Chemical Research (RIKEN), Wako-shi, 351-01 Saitama, Japan

Received 4 February 1999 and Received in final form 28 November 1999

Abstract. A non-orthogonal tight-binding molecular-dynamics formalism is used to simulate Raman spectra of the fullerene molecules C_{60} and C_{70}. Two parametrization schemes for the Hamiltonian and the overlap matrix elements are investigated. The considered molecules are excited randomly and the Fourier transform of the displacement autocorrelation function is employed to extract the vibrational properties. Fair agreement with experiment and with force-constant and *ab initio* calculations is achieved, with comparatively smaller maximum errors in the frequencies than for other molecular dynamics or semi-empirical calculations from the literature.

PACS. 31.15.Qg Molecular dynamics and other numerical methods – 71.20.Tx Fullerenes and related materials; intercalation compounds – 33.20.Fb Raman and Rayleigh spectra (including optical scattering)

1 Introduction

Among other traditional quantum chemical methods, tight-binding (TB) schemes have been successfully applied in the last two decades for the investigation of extended covalent systems [1–12]. TB schemes can be viewed as simplified two-center-oriented *ab initio* methods since the electronic properties of the system are determined quantum-mechanically. Their results deviate only slightly from those of more sophisticated methods, being obtained at reasonable computational costs.

At the center of many first-principles molecular-dynamics (MD) methods there has been the *a priori* theory based on universal parameters developed by Harrison [1]. This theory has been successful in describing covalent systems with tetrahedral coordination, however, it has proven to be less adequate for more general coordinations in systems dominated by multicenter bonds (also the case of fullerenes), for which the non-orthogonality of the atomic orbitals has to be taken into account. Van Schilfgaarde and Harrison [2] generalized the conventional TB approach such as to apply to non-tetrahedral and multicoordinated systems. This non-orthogonal theory was incorporated in the TB molecular dynamics (TBMD) formulation developed by Menon and Allen [3] and was successfully used to describe properties of carbon and silicon clusters [4–6].

An elaborate TB parametrization was developed by Cohen *et al.* [7] and Mehl *et al.* [8], wherein the parameters are chosen to reproduce both the first-principles total energy and electronic band structure of face-centered and body-centered cubic crystals. This method has been shown to work well for transition metals, predicting correctly besides electronic ground state properties also elastic constants, phonon frequencies, surface energies, and vacancy formation energies in agreement with experiment and first-principles results. A slightly modified version of this scheme was elaborated by Papaconstantopoulos *et al.* [9] and was successfully applied to carbon and silicon.

Another remarkable TB approach, intended to avoid the difficulties arising from an empirical parametrization of the Hamiltonian and overlap matrices is the density-functional tight-binding (DF-TB) approach of Porezag *et al.* [10–12]. Here the Hamiltonian and overlap matrices result out of a local orbital basis by using the density-functional theory local-density approximation and some integral approximations.

The interest in calculating Raman-spectra for fullerene molecules stems, on one hand, from the wealth of available experimental data and, on the other, from incompletely elucidated assignments (such as for C_{70}). Additionally, from a rather technical point of view, we are interested in evidencing the virtues of a yet insufficiently explored MD strategy based on autocorrelation functions, which appears to be very well suited for this purpose. We basically employ the TBMD formulation of Menon and Allen [3] to study the Raman-active modes of C_{60} and C_{70} by using comparatively for the Hamiltonian and overlap matrices the parametrization schemes of van Schilfgaarde and Harrison and of Papaconstantopoulos *et al.* The focus in using the first model is on adjusting the implied TB parameters for optimal description of structural and

[a] On leave from the University of Cluj-Napoca, Department of Theoretical Physics, 3400 Cluj-Napoca, Romania.
e-mail: tbeu@phys.ubbcluj.ro

vibrational properties. As for the second model, the aim is to investigate its quality (proven in describing other properties) for simulating Raman-spectra of fullerenes, with a view to treating accurately higher fullerenes or fullerene aggregates. As will clearly follow from the present study, a high quality parametrization of the Hamiltonian and overlap matrices can make a TBMD approach comparable to *ab initio* methods concerning the accuracy, and definitely more economical regarding the computational effort.

In Section 2 we give a brief outline of the used non-orthogonal TBMD formalism. In Section 3 the two employed TB parametrization schemes are presented, and, finally, Section 4 is devoted to the description of the obtained results and to comparisons with other reported results.

2 Non-orthogonal tight-binding MD

MD simulations generally imply numerically solving Newton's equation for all N atoms in the considered structure:

$$m\ddot{\mathbf{R}}_I = \mathbf{F}_I, \quad I = 1, N.$$

The forces acting on the atoms can be expressed as derivatives of the total energy $E_{\rm tot}(\{\mathbf{R}_J\})$ of the system with respect to the individual position vectors $\mathbf{R}_I$:

$$\mathbf{F}_I = -\frac{\partial E_{\rm tot}(\{\mathbf{R}_J\})}{\partial \mathbf{R}_I}\,.$$

The total energy of the system can be approximated by the sum between the electronic contribution (calculated quantum-mechanically as the sum of one-electron energies) and a short-range repulsive two-body potential:

$$\begin{aligned} E_{\rm tot}(\{\mathbf{R}_J\}) &= E_{\rm el}(\{\mathbf{R}_J\}) + E_{\rm rep}(\{|\mathbf{R}_J - \mathbf{R}_K|\}) \\ &= \sum_{k=1}^{n_{\rm occ}} n_k \varepsilon_k(\{\mathbf{R}_J\}) + \sum_{J<K}\sum V_{\rm rep}(|\mathbf{R}_J - \mathbf{R}_K|). \quad (1) \end{aligned}$$

In the case of sp^3 bonding, the total number of electrons is $n = 4N$, the number of occupied one-electron states is $n_{\rm occ} = n/2$, and their occupation number is $n_k = 2$.

The electronic contributions ε_k to the total energy result as eigenvalues of the characteristic equation:

$$(\mathbf{H} - \varepsilon_k \mathbf{S})\mathbf{C}^k = 0,$$

where the Hamiltonian matrix, $\mathbf{H}$, and the overlap matrix, $\mathbf{S}$, are expressed in the representation of some non-orthogonal set of atom-centered orbitals. The column vector $\mathbf{C}^k$ is the eigenvector corresponding to eigenvalue ε_k. The gradient of the eigenvalues, necessary for calculating the forces, can be readily obtained by taking the gradient of the characteristic equation and multiplying on the left with $\mathbf{C}^{k\dagger}$. The total force acting upon atom I then takes the form:

$$\mathbf{F}_I = -\sum_{k=1}^{n_{\rm occ}} \frac{n_k}{\mathbf{C}^{k\dagger}\mathbf{S}\mathbf{C}^k}\mathbf{C}^{k\dagger}\left(\frac{\partial \mathbf{H}}{\partial \mathbf{R}_I} - \varepsilon_k \frac{\partial \mathbf{S}}{\partial \mathbf{R}_I}\right)\mathbf{C}^k - \frac{\partial E_{\rm rep}}{\partial \mathbf{R}_I}\,. \quad (2)$$

Within the orthogonal TB formalism of Harrison [1], bond orbitals are constructed from sp^3 hybrids for the tetrahedral structure. The use of sp^3 bonding for fullerenes is justified by the fact that the nominal sp^2 bonding between adjacent carbon atoms actually occurs on a curved surface, which leads to some admixture of sp^3 bonding. The $4N \times 4N$ Hamiltonian matrix for the system of the valence electrons can be viewed as being composed of 4×4 blocks corresponding to the coupling between the s, p_x, p_y and p_z orbitals of the involved atoms:

$$\mathbf{H} = \begin{array}{c} \overbrace{}^{\text{atom } I} \quad \overbrace{}^{\text{atom } J} \\ \begin{matrix} s^I & p_x^I & p_y^I & p_z^I & & s^J & p_x^J & p_y^J & p_z^J \end{matrix} \\ \begin{bmatrix} \ddots & \vdots & & \vdots & & \vdots & & & \vdots & \\ \cdots & h_s^I & 0 & 0 & 0 \cdots & H_{ss}^{IJ} & H_{sx}^{IJ} & H_{sy}^{IJ} & H_{sz}^{IJ} & \cdots \\ & 0 & h_p^I & 0 & 0 & -H_{sx}^{IJ} & H_{xx}^{IJ} & H_{xy}^{IJ} & H_{xz}^{IJ} & \\ & 0 & 0 & h_p^I & 0 & -H_{sy}^{IJ} & H_{xy}^{IJ} & H_{yy}^{IJ} & H_{yz}^{IJ} & \\ \cdots & 0 & 0 & 0 & h_p^I \cdots & -H_{sz}^{IJ} & H_{xz}^{IJ} & H_{yz}^{IJ} & H_{zz}^{IJ} & \cdots \\ & \vdots & & \vdots & \ddots & \vdots & & & \vdots & \end{bmatrix} \begin{matrix} s^I \\ p_x^I \\ p_y^I \\ p_z^I \end{matrix} \end{array}.$$

In a simplified model, the diagonal *on-site* elements h_l^I ($l = s$ or p) can be attributed the significance of atomic energies, but in general they should be allowed to vary depending upon the local environment of each atom. For the Hamiltonian matrix elements of the non-diagonal block (I, J) the Slater-Koster form is usually considered [13]. In terms of bond direction cosines (γ_x^{IJ}, γ_x^{IJ} and γ_x^{IJ}) and two-center *hopping parameters* ($H_{ss\sigma}$, $H_{sp\sigma}$, $H_{pp\sigma}$, $H_{pp\pi}$), the relevant elements are expressed as:

$$\begin{cases} H_{ss}^{IJ} = H_{ss\sigma}^{IJ}, \\ H_{sx}^{IJ} = \gamma_x^{IJ} H_{sp\sigma}^{IJ}, \\ H_{xy}^{IJ} = \gamma_x^{IJ}\gamma_y^{IJ}\left(H_{pp\sigma}^{IJ} - H_{pp\pi}^{IJ}\right) + H_{pp\sigma}\delta_{xy}, \end{cases}$$

the rest of them resulting by straightforward changes of indices x, y and z. Here $\delta_{\alpha\beta}$ is the Kronecker symbol.

Within a non-orthogonal TB formalism, the overlap matrix has a form similar to the Hamiltonian, but with the diagonal on-site terms equal to 1 and the elements of the non-diagonal blocks expressed in terms of the corresponding hopping parameters ($S_{ss\sigma}$, $S_{sp\sigma}$, $S_{pp\sigma}$, $S_{pp\pi}$).

3 Parametrization models

The first parametrization we consider for the Hamiltonian and overlap matrices, denoted hereafter as "model I", is based on the TB theory developed by van Schilfgaarde and Harrison [2] for covalent multicoordinated systems

with non-tetrahedral coordination. The atoms are characterized only by their valence energies, covalent radii and universal interaction parameters (primitive TB matrix elements $V_{ll'\mu}$), which are transferable. The problem of calculating the overlap matrix elements was solved by assuming a proportionality between **H** and **S** (analogously to the extended Hückel theory).

In this approach, the diagonal on-site Hamiltonian elements h_l^I $(l = s, p)$ are environment independent, being identified with atomic energies:

$$h_s^I = \varepsilon_s, \quad h_p^I = \varepsilon_p.$$

The Slater-Koster hopping terms $H_{ll'\mu}$ and $S_{ll'\mu}$ are expressed in terms of primitive TB matrix elements $V_{ll'\mu}^{IJ}$ as:

$$H_{ll'\mu}^{IJ} = V_{ll'\mu}^{IJ}\left[1 + 1/K - \left(S_2^{IJ}\right)^2\right],$$
$$S_{ll'\mu}^{IJ} = \frac{2V_{ll'\mu}^{IJ}}{K(\varepsilon_l + \varepsilon_{l'})},$$

where for carbon only parameters $(ll'\mu) = (ss\sigma)$, $(sp\sigma)$, $(pp\sigma)$ and $(pp\pi)$ need to be considered. K is the Hückel proportionality constant and S_2^{IJ} is the non-orthogonality between sp^3 hybrids, given by:

$$S_2^{IJ} = \frac{1}{4}\left(S_{ss\sigma}^{IJ} - 2\sqrt{3}S_{sp\sigma}^{IJ} + S_{pp\sigma}^{IJ}\right).$$

We assume the TB matrix elements $V_{ll'\mu}^{IJ}$ to scale exponentially with the interatomic separation R_{IJ}:

$$V_{ll'\mu}^{IJ}(R_{IJ}) = V_{ll'\mu}\exp\left[-\alpha_\mu\left(R_{IJ} - R_0\right)\right], \qquad (3)$$

with their equilibrium values resulting from the prescriptions of Harrison's theory [1]. R_0 is a parameter with the significance of an equilibrium distance, which in our calculations is taken equal to the average of the experimentally determined bond distances. The exponential parameters α_σ and α_π directly relate to the longitudinal and transverse bond-stretching force constants and thus can be fitted to reproduce vibrational frequencies.

The short-range repulsive pair potential is modeled to scale exponentially with distance, as well:

$$V_{\rm rep}(R_{IJ}) = V_{\rm rep}^0\exp\left[-\beta\left(R_{IJ} - R_0\right)\right], \qquad (4)$$

where, by similar arguments to those of Menon and Allen [3], we take β to be twice the weighted average of the α_μ parameters, *i.e.* $\beta = (\alpha_\sigma + 3\alpha_\pi)/2$.

The TB parameters ε_s, ε_p, $V_{ss\sigma}$, $V_{sp\sigma}$, $V_{pp\sigma}$ and $V_{pp\pi}$ employed in our calculations as part of model I are listed in Table 1 and do not actually originate in the universal parameter scheme of Harrison [1], but are the ones reported by Chadi and Martin [14]. We take R_0 to be approximately equal to the average of the experimental single and double bond lengths of C_{60} ($a_5 = 1.455$ Å and $a_6 = 1.391$ Å, respectively [15]). For the Hückel constant K, the value suggested in reference [4] was considered and the results seem to be very little sensitive to this parameter. As for the exponential parameters α_σ and α_π, the optimal values for describing the experimental Raman spectra of C_{60} and C_{70} have been found to be $1.80/R_0$ and $2.20/R_0$, respectively. Finally, the repulsive parameter $V_{\rm rep}^0$ was adjusted such as to reproduce the geometrical properties of the C_{60} cage (average radius and bond lengths). α_σ, α_π and $V_{\rm rep}^0$ are alike consistent with values resulted from exponential fits to the C–C interaction reported by Porezag *et al.* [10].

Table 1. Parameters employed in model I (ε_s, ε_p, $V_{ss\sigma}$, $V_{sp\sigma}$, $V_{pp\sigma}$ and $V_{pp\pi}$ are from Chadi and Martin [14]).

ε_s	−17.52 eV	$V_{ss\sigma}$	−5.55 eV	α_σ	$1.80/R_0$
ε_p	−10.72 eV	$V_{sp\sigma}$	5.91 eV	α_π	$2.20/R_0$
K	2.1	$V_{pp\sigma}$	7.78 eV	β	$\frac{1}{2}(\alpha_\sigma + 3\alpha_\pi)$
R_0	1.42 Å	$V_{pp\pi}$	−2.50 eV	$V_{\rm rep}^0$	1 eV

The second considered parametrization, denoted hereafter as "model II", is the TB total energy method of Papaconstantopoulos *et al.* [9]. Here, the environment of each individual atom is determined by a pseudo-atomic density:

$$\rho_I = \sum_{J\neq I}^{N}\exp\left(-\lambda^2 R_{IJ}\right) f(R_{IJ}),$$

depending on the distances to all neighbors exponentially and through a cutoff function defined as:

$$f(R) = \left\{1 + \exp\left[(R - R_{\rm c})/\Delta\right]\right\}^{-1}.$$

The cutoff is chosen such that $f(R)$ practically vanishes when $R > R_{\rm c}$, the main decrease taking place roughly within a domain of size Δ. For carbon the values $R_{\rm c} = 10.5a_0$ and $\Delta = 0.5a_0$ are employed (with a_0 the Bohr radius).

The on-site Hamiltonian elements are given in terms of the local pseudo-atomic density by a Birch-like equation:

$$h_l^I = \alpha_l + \beta_l\rho_I^{2/3} + \gamma_l\rho_I^{4/3} + \chi_l\rho_I^2,$$

where, obviously, only $l = s, p$ are considered. As for the two-center Slater-Koster hopping terms, they have been parametrized as polynomials times an exponential cutoff in order to exhibit the proper behavior for small interatomic distances:

$$H_{ll'\mu}(R) = \left(a_{ll'\mu} + b_{ll'\mu}R + c_{ll'\mu}R^2\right)\exp\left(-d_{ll'\mu}^2 R\right) f(R)$$
$$S_{ll'\mu}(R) = \left(\delta_{ll'} + p_{ll'\mu}R + q_{ll'\mu}R^2 + r_{ll'\mu}R^3\right)$$
$$\times\exp\left(-s_{ll'\mu}^2 R\right) f(R).$$

Here again, only parameters $(ll'\mu) = (ss\sigma)$, $(sp\sigma)$, $(pp\sigma)$ and $(pp\pi)$ are considered. There is no explicit repulsive contribution $V_{\rm rep}$ as part of this parametrization and all relevant coefficients are listed in Table 1 of reference [9].

The interatomic forces for both models can be expressed analytically according to equation (2), and this is an essential aspect in performing tractable MD simulations.

4 Results and discussion

For both considered fullerene molecules, C_{60} and C_{70}, we performed MD simulations based on both models I and II. Typically, the initial configuration was prepared by displacing the atoms randomly relative to their equilibrium positions. Nevertheless, to excite particular groups of vibrational modes, also certain restricted initial displacement patterns have been applied.

In order to characterize the overall vibration of the investigated molecules, we employed the *displacement* autocorrelation function (DAF):

$$C_{\delta\mathbf{r}}(t) = \sum_{I=1}^{N} \langle \delta\mathbf{r}_I(t) \cdot \delta\mathbf{r}_I(0) \rangle.$$

Alternatively, the usefulness of the *position* autocorrelation function (PAF),

$$C_{\mathbf{r}}(t) = \sum_{I=1}^{N} \langle \mathbf{r}_I(t) \cdot \mathbf{r}_I(0) \rangle,$$

was also examined. $C_{\delta\mathbf{r}}(t)$ was generally found to be more sensitive to the individual normal modes than $C_{\mathbf{r}}(t)$ and its more meaningful Fourier-transform (FT) spectrum was consequently used in all comparisons with experimental spectra.

The vibration of a molecule with an inversion point (such as C_{60}) can be characterized, additionally, by the *parity*, which we define as:

$$P = \frac{\sum_{I=1}^{N} \langle \delta\mathbf{r}_I \cdot (-\delta\mathbf{r}_{\mathrm{sym}(I)}) \rangle}{\sum_{I=1}^{N} (\delta\mathbf{r}_I)^2},$$

where $\mathrm{sym}(I)$ designates the symmetrical atom for atom I. Since, as it is well-known, the 10 Raman-active vibrations of C_{60} have *gerade* symmetry ($2A_g + 8H_g$), while the 4 IR-active modes have *ungerade* symmetry (F_{1u}), monitoring the parity of the vibration can yield essential information about the nature of the obtained FT spectrum.

Our calculated electronic levels for C_{60} are in good agreement with those found from other calculations [16] and reproduce the main features of experimental data [17]. The ground-state electronic structure ($3a+10t+8g+11h$) is preserved and the total energy conserved throughout the simulation.

Figure 1 shows the time dependence of various characteristic geometrical quantities of C_{60} monitored during a typical run: the DAF and PAF, the minimum and maximum cage radii, $R_{\min}$ and $R_{\max}$, and the parity of the vibration. In all simulations a time step of 2×10^{-4} picoseconds was employed and up to a total of 14 000 steps were performed. The graphs of Figure 1 actually depict only the first picosecond of a run based on model II with random initial excitation. Qualitatively, similar results have been also obtained for model I, which will be seen, however, to yield poorer agreement with the experiment.

As can be easily noticed, the behavior of $C_{\mathbf{r}}(t)$ is qualitatively different from the one of $C_{\delta\mathbf{r}}(t)$, following closely

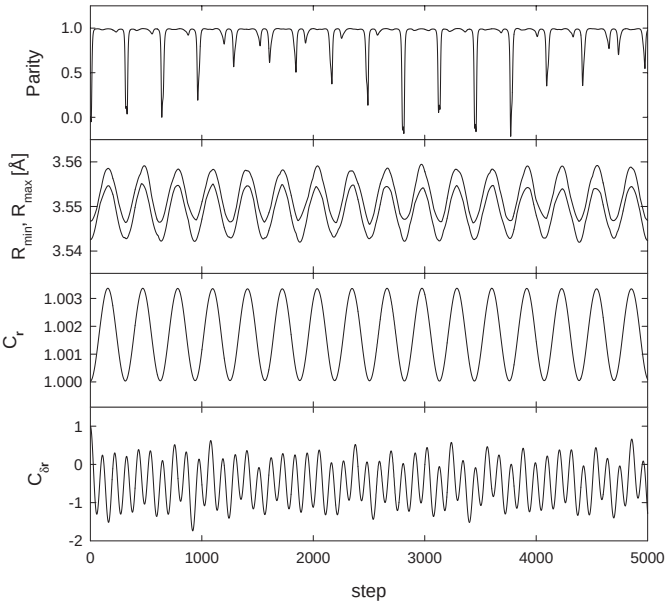

Fig. 1. Time dependence of various quantities monitored during a typical run for C_{60} by using model II; $C_{\delta r}$: displacement autocorrelation function, $C_{\mathbf{r}}$: position autocorrelation function, $R_{\min}$ and $R_{\max}$: minimum and maximum C_{60} cage radii. The time step equals 2×10^{-16} s.

the simple periodicity of $R_{\min}$ and $R_{\max}$. This clearly indicates the domination of $C_{\mathbf{r}}(t)$ by the low-frequency primarily radial modes. As a consequence, the FT spectrum of $C_{\mathbf{r}}(t)$ generally contains limited information, basically showing a single peak corresponding to the totally symmetrical "breathing" mode $A_g(1)$ (at 493 cm^{-1} [18]). As a matter of fact, for C_{70}, too, the PAF has proven to be useful *only* for unambiguously positioning the symmetrical breathing mode A_1'.

For a random initial excitation of C_{60}, the normalized parity of the vibration can be seen to be predominantly positive, typically exceeding 0.9 on the average, which implies that the composite vibration of the molecule has overwhelmingly *gerade* symmetry. This behavior is actually a direct result of the *uniform* character of the applied random excitation and, for our approach, it has the important consequence that the FT spectrum of the DAF can be directly related to the experimental Raman-spectrum. The parity decreases only when the C_{60} cage shrinks to its minimum size ($R_{\min}$ and $R_{\max}$ reach their minimum).

Figure 2 shows along with the experimental Raman spectrum obtained by Eklund *et al.* [18] for a pristine C_{60} film, typical FT spectra of the DAF calculated by using the parametrizations of models I and II, respectively, and random initial excitation. The scaling factors applied to the simulated spectra are 0.83 for model I and 0.95 for model II. Besides the almost unitary scaling factor, one can also notice the much better agreement of the peaks yielded by model II with the experiment, both regarding position and amplitude. The superior quality of model II (parametrization of Ref. [9]) is obviously a direct consequence of the more appropriate form of the on-site and

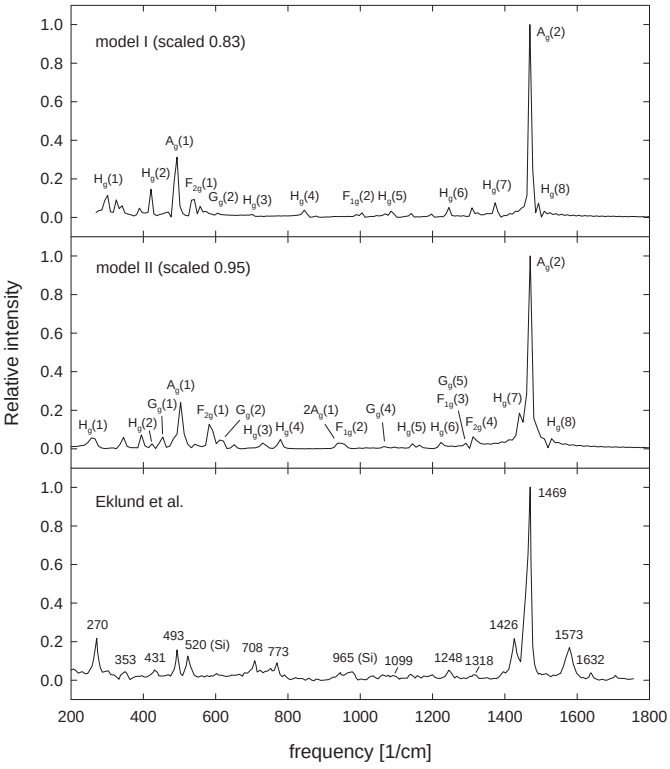

Fig. 2. Experimental Raman spectrum for C_{60} (Ref. [18]) and FT spectra of the displacement autocorrelation function calculated with models I and II.

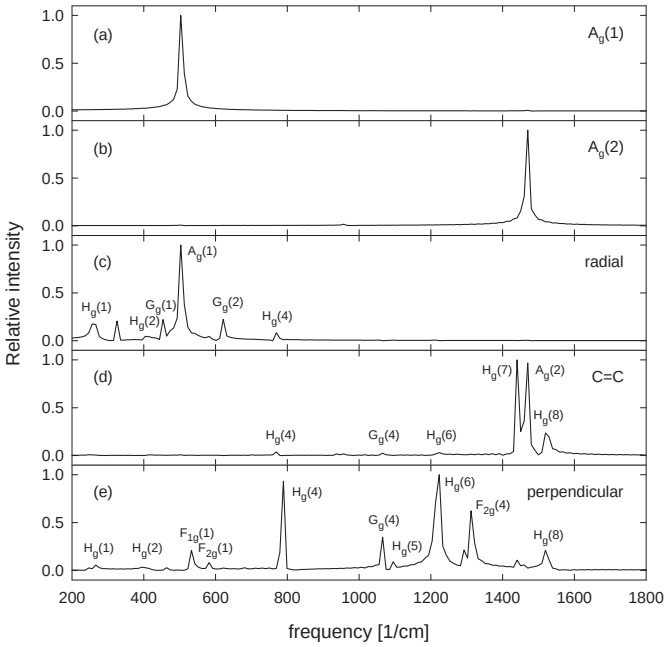

Fig. 3. FT spectra of the displacement autocorrelation function for C_{60} calculated with models I and II for various initial excitation patterns: (a) radial "breathing" displacement, (b) tangential "pentagonal pinch" displacement, (c) random displacement along the radial direction, (d) random displacement along a direction perpendicular to the radius and in the plane formed by the C=C bond and the radius, (e) random displacement along the tangential direction perpendicular to the radius and the C=C bond.

hopping terms and of the richer information used to fit its parameters.

Since by its specific nature our approach does not deal with individual vibrational modes separately, in order to unambiguously assign the peaks obtained for C_{60}, besides the totally random excitation, we also employed several restricted initial excitation patterns, whose FT spectra are plotted in Figure 3. The simplest among these patterns, yielding the $A_g(1)$ peak shown in panel (a), implies the radially symmetrical in-phase displacement of all atoms. The tangential "pentagonal pinch" mode $A_g(2)$, corresponding to the peak of panel (b), was excited by the in-phase elongation of all C=C bonds.

The spectra of panels (c), (d) and (e) involve, respectively, initial displacements along one of the three reciprocally orthogonal local coordinates of each atom (one radial and two tangential). The spectrum of the predominantly *radial* modes depicted in panel (c) originates in random displacements along the radial direction and it includes, in particular, the $A_g(1)$ vibration, too. The peaks of panel (d) were obtained by random displacements along the tangential direction perpendicular to the radius and *in the plane* formed by the C=C bond and the radius. Finally, the peaks composing spectrum (e) imply random displacements along the tangential direction *perpendicular* to the radius and the C=C bond.

The orthogonality of the radial and tangential local coordinates of the atoms allows one to characterize each vibrational mode by percentage contributions from each of the three directions. From this perspective, the assignment of the peaks of panels (c), (d) and (e) was greatly facilitated by the analysis of Stanton and Newton [19], regarding the character of the individual normal modes of C_{60}.

The frequencies resulted from our calculations with model II (which is seen to reproduce more accurately the experimental evidence than model I) are listed in Table 2, along with the experimental Raman frequencies of Eklund *et al.* [18]. The relative differences $\Delta\nu/\nu_{\rm exp}$ of our frequencies with respect to the experimental values are compared with the corresponding differences resulted from four other representative calculations: the force-constant model calculations of Jishi *et al.* [20], the SCF-LDA calculations of Quong *et al.* [21], the DF-TB calculations of Porezag *et al.* [10], and the MNDO calculations of Fanti *et al.* [22]. We have additionally included the relative differences $\Delta\nu^*/\nu_{\rm exp}$ of the *scaled* frequencies yielded by model II ($\nu^* = 0.95\nu$). Whereas the agreement of the results of Jishi *et al.* and Quong *et al.* with the experiment is clearly better as compared to our unscaled frequencies, the errors of our scaled values seem to be comparable, in certain cases even smaller. There is just one vibrational mode, $H_g(5)$, which slightly departs from this behavior, with an associated relative difference of 4.2%. Moreover, even for our *unscaled* results one can easily notice the overall better agreement as compared to the calculations

Table 2. Experimental and calculated Raman frequencies (in cm^{-1}) for the fullerene cluster C_{60}. $\Delta\nu/\nu_{exp}$ are relative differences (in %) with respect to the experimental values of Eklund *et al.* $\Delta\nu^*/\nu_{exp}$ are the relative differences of the scaled frequencies resulted from model II (with a scaling factor of 0.95).

Mode	Eklund[a]	model II			Jishi[b]	Quong[c]	Porezag[d]	Fanti[e]
	ν_{exp}	ν	$\Delta\nu/\nu_{exp}$	$\Delta\nu^*/\nu_{exp}$	$\Delta\nu/\nu_{exp}$	$\Delta\nu/\nu_{exp}$	$\Delta\nu/\nu_{exp}$	$\Delta\nu/\nu_{exp}$
$H_g(1)$	270	280	3.7	−1.5	−0.4	−4.4	0.4	−2.3
$H_g(2)$	431	447	3.7	−1.5	1.9	1.9	0.7	8.4
$A_g(1)$	493	530	7.5	2.1	−0.2	−3.0	12.0	23.7
$H_g(3)$	708	769	8.6	3.2	0.0	2.7	0.8	8.9
$H_g(4)$	773	820	6.1	0.8	1.9	−0.8	12.3	19.5
$H_g(5)$	1099	1205	9.6	4.2	0.3	−0.5	13.5	14.6
$H_g(6)$	1248	1288	3.2	−2.0	−2.5	−0.3	15.0	12.7
$H_g(7)$	1426	1516	6.3	1.0	−1.8	1.2	14.7	11.9
$A_g(2)$	1469	1548	5.4	0.1	−0.1	2.0	14.6	13.5
$H_g(8)$	1573	1610	2.4	−2.8	0.1	0.2	15.1	9.3

[a] Ref. [18] (measured for pristine C_{60} film). [b] Ref. [20] (force-constant model). [c] Ref. [21] (SCF-LDA calculation). [d] Ref. [10] (DF-TB calculation). [e] Ref. [22] (MNDO calculation).

of Porezag *et al.* and Fanti *et al.* For the $A_g(2)$ mode, for example, our unscaled results lie by approximately 9 and, respectively, 8% in better agreement. The explanation for the more favorable behavior in comparison with the results of Porezag *et al.*, which basically originate in a TBMD approach, too, is to be sought in the more realistic parametrization of Papaconstantopoulos *et al.*, with higher experimental significance, on which our model II relies. Thus, even though the crude frequencies calculated with model II are somewhat less accurate as compared to existing force-constant or SCF-LDA results, they are, however, superior to other TB and MNDO results.

The methodology for investigating C_{60} was also applied to the simulation of geometrical and vibrational properties of the C_{70} molecule. However, due to the lower symmetry, the assignment of the 53 Raman-active modes of C_{70} is much more difficult than in the case of C_{60}. There have been several attempts [20,23–28], nevertheless an unambiguous assignment scheme has not met general consensus yet (see, for example, Ref. [26]).

The initial excitation of the system was achieved, as before, by random displacements of the atoms. To excite particular modes (as, for example, the two A_1' vibrations at 452 and 1446 cm^{-1}, identified as analogous to the totally symmetrical breathing and pentagonal pinch modes of C_{60}, respectively), separate runs with deterministic initial displacement patterns have been performed. The FT spectra of the DAF obtained by using models I and II, along with the experimental Raman spectrum of Brockner *et al.* [23], are depicted in Figure 4. It is worth mentioning that the optimal scaling factors for both models have been found to be the same as in the case of C_{60} (0.83 and 0.95, respectively). Again the superiority of model II is apparent, both by the scaling factor closer to unity and the better agreement with the experimental peak positions and intensities.

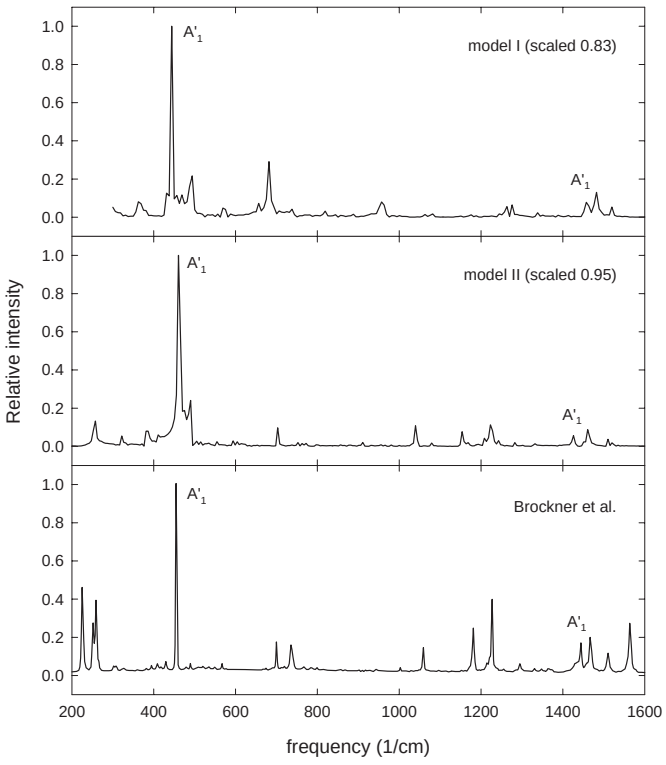

Fig. 4. Experimental Raman spectrum for C_{70} (Ref. [23]) and FT spectra of the displacement autocorrelation function calculated with models I and II.

The fair agreement of the scaled frequencies ($\nu^* = 0.95\nu$) with the experiment can also be judged from Table 3, where the most intense 20 peaks in our spectrum for model II have been included. In addition, the relative differences with respect to the experimental frequencies, $\Delta\nu^*/\nu_{exp}$, seen to amount to less than 4% (excepting the vibration at 302 cm^{-1}), are compared

Table 3. Experimental and calculated frequencies (in cm^{-1}) for the 20 most intense Raman-active modes of the fullerene cluster C_{70}. $\Delta\nu/\nu_{exp}$ are relative differences (in %) with respect to the experimental values of Brockner *et al.* ν^* are the scaled frequencies resulted from model II with a scaling factor of 0.95. The assignment scheme of Wang *et al.* is used.

Mode	Brockner[a]	model II		Jishi[b]	Wang[c]	Onida[d]
	ν_{exp}	ν^*	$\Delta\nu^*/\nu_{exp}$	$\Delta\nu/\nu_{exp}$	$\Delta\nu/\nu_{exp}$	$\Delta\nu/\nu_{exp}$
A_1'	259	257	−0.8	0.4	1.2	−3.5
E_2'	302	322	6.6		−5.0	3.0
A_1'	394	381	−3.3	−11.7	−1.5	2.0
E_1''	409	411	0.5	1.5	0.0	2.4
A_1'	454	460	1.3	1.3	0.4	2.4
E_2'	490	490	0.0	−3.1	1.6	6.1
A_1'	567	555	−2.1	−2.1	4.6	5.8
E_1''	700	703	0.4	0.7	0.6	8.6
E_1''	736	753	2.3	0.1	0.5	3.7
E_1''	767	772	0.7	3.8	0.7	7.3
E_1''	799	797	−0.3	0.8	−0.4	33.2
E_2'	943	956	1.4		0.1	12.1
A_1'	1059	1040	−1.8	1.0	−2.8	1.0
E_1''	1181	1154	−2.3	0.1	1.0	4.2
E_2'	1227	1223	−0.3	−2.0	0.4	2.0
E_1''	1295	1282	−1.0	0.8	−0.5	−0.8
E_2'	1331	1332	0.1	0.3	0.5	5.1
A_1'	1444	1426	−1.2	−2.0	−1.0	7.1
E_1''	1467	1461	−0.4	1.1	0.4	2.1
E_1''	1510	1510	0.0	2.0	0.8	3.6

[a] Ref. [23] (experiment). [b] Ref. [20] (force-model calculation). [c] Ref. [27] (LDA calculation). [d] Ref. [28] (Car-Parrinello MD calculation).

with the corresponding differences resulted from the force-constant calculations of Jishi *et al.* [20], the LDA calculations of Wang *et al.* [27] and the Car-Parrinello MD calculations of Onida *et al.* [28]. Aside from the vibrations at 302 and 394 cm^{-1}, showing for one or the other approaches higher deviations from the experiment, our results are of comparable accuracy with those of Jishi *et al.* and Wang *et al.* As for the calculations of Onida *et al.*, the results are obviously affected by higher inaccuracies than for any of the other compared approaches. It should be also mentioned, that the MNDO calculations of Raghavachari *et al.* [29] are reported to show typical frequency deviations of up to 15%. Thus, analogous to the investigation of C_{60}, the scaled frequencies calculated with model II are comparable in accuracy with existing force-constant and LDA results and they are definitely superior to other MD and MNDO results.

5 Conclusions

A non-orthogonal TBMD approach is employed to simulate structural properties and Raman spectra of C_{60} and C_{70}. Non-orthogonality is confirmed to play an essential role in the case of carbon clusters since its explicit inclusion has beneficial effects on the agreement of the obtained results with the experimental data.

Two parametrizations schemes for the Hamiltonian and overlap matrices are investigated comparatively. The first one, denoted as "model I", originates in the *a priori* theory based on universal parameters developed by Harrison [1] and improved by van Schilfgaarde and Harrison [2]. The primitive electronic tight-binding matrix elements $V_{ll'\mu}^{IJ}$ are assumed to scale exponentially with the interatomic separation and the exponential factors (which relate to bond-stretching force constants) are adjusted such as to optimally reproduce geometric properties and the frequencies of the Raman-active modes of C_{60} and C_{70}.

The second parametrization, denoted as "model II", is the one of Papaconstantopoulos *et al.* [9]. It involves environment-dependent on-site terms (by defining a local pseudo-atomic density) and it models the Hamiltonian and overlap matrices as polynomials times an exponential cutoff with respect to the interatomic separation.

The initial excitation of the investigated fullerene molecules is carried out by random initial displacements of all atoms, or, in order to excite vibrational modes from particular frequency regions, by certain restricted displacement patterns. To characterize the overall vibration of the molecules, the autocorrelation function

of the individual atomic displacements is employed and its Fourier-transform is matched against experimental Raman-spectra.

As compared to model I, the calculated spectra for model II are in obviously better agreement with the experimental evidence both for C_{60} and C_{70}, and this is due to the high quality data used to adjust the parametrization of Papaconstantopoulos *et al.* Moreover, even though the accuracy of our unscaled frequencies is slightly inferior to other force-constant and LDA models, it turns out, however, to be superior to other MD and semi-empirical calculations.

We have achieved fair agreement with experiment both for structural and vibrational properties. The average cage sizes and average bond lengths are in less than 2% error, the relative differences between our unscaled vibrational frequencies and the experimental data amounting to less than 10%.

References

1. W. Harrison, *Electronic Structure and the Properties of Solids* (Freeman, San Francisco, 1980).
2. M. van Schilfgaarde, W.A. Harrison, J. Phys. Chem. Solids **46**, 1093 (1985).
3. M. Menon, R.E. Allen, Phys. Rev. B **38**, 6196 (1988).
4. M. Menon, K.R. Subbaswamy, Phys. Rev. Lett. **67**, 3487 (1991).
5. M. Menon, K.R. Subbaswamy, Phys. Rev. B **47**, 12754 (1993); Phys. Rev. B **48**, 8398 (1993).
6. M. Menon, K.R. Subbaswamy, M. Sawtarie, Phys. Rev. B **49**, 13966 (1994).
7. R.E. Cohen, M.J. Mehl, D.A. Papaconstantopoulos, Phys. Rev. B **50**, 14694 (1994)
8. M.J. Mehl, D.A. Papaconstantopoulos, Phys. Rev. B **54**, 4519 (1996).
9. D.A. Papaconstantopoulos, M.J. Mehl, S.C. Erwin, M.R. Pederson, Mat. Res. Soc. Symp. Proc. **491**, 221 (1998).
10. D. Porezag, Th. Frauenheim, Th. Köhler, G. Seifert, R. Kaschner, Phys. Rev. B **51**, 12947 (1995).
11. D. Porezag, M.R. Pederson, Th. Frauenheim, Th. Köhler, Phys. Rev. B **52**, 14963 (1995).
12. D. Porezag, Th. Frauenheim, Carbon **37**, 463 (1999).
13. J.C. Slater, G.F. Koster, Phys. Rev. **94**, 1498 (1954).
14. D.J. Chadi, R.M. Martin, Solid State Commun. **19**, 643 (1976).
15. M.S. Dresselhaus, G. Dresselhaus, P.C. Eklund, *Science of Fullerenes and Carbon Nanotubes* (Academic Press, San Diego, 1996), pp. 60-61 and references therein.
16. J.W. Mintmire, B.I. Dunlap, D.W. Brenner, R.C. Mowrey, C.T. White, Phys. Rev. B **43**, 14281 (1991).
17. D.L. Lichtenberger, K.W. Nebesny, C.D. Ray, D.R. Huffman, L.D. Lamb, Chem. Phys. Lett. **176**, 203 (1991).
18. P.C. Eklund, A.M. Rao, Y. Wang, P. Zhou, K.A. Wang, J.M. Holden, M.S. Dresselhaus, G. Dresselhaus, Thin Solid Films **257**, 211 (1995).
19. E. Stanton, M.D. Newton, J. Phys. Chem. **92**, 2141 (1988).
20. R.A. Jishi, R.M. Mirie, M.S. Dresselhaus, G. Dresselhaus, P.C. Eklund, Phys. Rev. B **48**, 5634 (1994).
21. A.A. Quong, M.R. Pederson, J.L. Feldman, Solid State Commun. **87**, 535 (1993).
22. M. Fanti, G. Orlandi, F. Zerbetto, J. Phys. B: At. Mol. Phys. **29**, 5065 (1996).
23. W. Brockner, F. Menzel, J. Mol. Struct. **378**, 147 (1996).
24. K. Lynch, C. Tanke, F. Menzel, W. Brockner, P. Scharff, E. Stumpp, J. Phys. Chem. **99**, 7985 (1995).
25. S.H. Gallagher, R.S. Armstrong, R.D. Bolskar, P.A. Lay, C.A. Reed, J. Am. Chem. Soc. **119**, 4263 (1997).
26. S.H. Gallagher, R.S. Armstrong, R.D. Bolskar, P.A. Lay, C.A. Reed, J. Mol. Struct. **407**, 81 (1997).
27. X.Q. Wang, C.Z. Wang, K.M. Ho, Phys. Rev. B **51**, 8656 (1995).
28. G. Onida, W. Andreoni, J. Kohanoff, M. Parrinello, Chem. Phys. Lett. **219**, 1 (1994).
29. K. Raghavachari, C.M. Rohlfing, J. Phys. Chem. **95**, 5768 (1991).